Phys Chem Minerals (2004) 31: 375–385
DOI 10.1007/s00269-004-0402-2

ORIGINAL PAPER

G. Iezzi · F. Cámara · G. Della Ventura · R. Oberti
G. Pedrazzi · J-L. Robert

Synthesis, crystal structure and crystal chemistry of ferri-clinoholmquistite, $\square Li_2Mg_3Fe^{3+}{}_2Si_8O_{22}(OH)_2$

Received: 2 December 2003 / Accepted: 30 April 2004

Abstract This work reports the synthesis of ferri-clinoholmquistite, nominally $\square_{Li2}(Mg_3Fe^{3+}{}_2)Si_8O_{22}(OH)_2$, at varying f_{O_2} conditions. Amphibole compositions were characterized by X-ray (powder and single-crystal) diffraction, microchemical (EMPA) and spectroscopic (FTIR, Mössbauer and Raman) techniques. Under reducing conditions ($\leq$ NNO + 1, where NNO = Nickel–Nickel oxide buffer), the amphibole yield is very high (> 90%), but its composition, and in particular the FeO/Fe_2O_3 ratio, departs significantly from the nominal one. Under oxidizing conditions ($\leq$ NNO + 1.5), the amphibole yield is much lower (< 60%, with Li-pyroxene abundant), but its composition is close to the ideal stoichiometry. The exchange vector of relevance for the studied system is $^{M2}(Mg,Fe^{2+})$ $^{M4}(Mg,Fe^{2+})$ $^{M2}Fe^{3+}{}_{-1}$ $^{M4}Li_{-1}$, which is still rather unexplored in natural systems. Amphibole crystals of suitable size for structure refinement were obtained only at 800 °C, 0.4 GPa and NNO conditions (sample 152), and have $C2/m$ symmetry. The X-ray powder patterns for all other samples were indexed in the same symmetry; the amphibole closest to ideal composition has a = 9.428(1) Å, b = 17.878(3) Å, c = 5.282(1) Å, β = 102.06(2)°, V = 870.8(3) Å^3. Mössbauer spectra show that Fe^{3+} is strongly ordered at M2 in all samples, whereas Fe^{2+} is disordered over the B and C sites. FTIR analysis shows that the amount of $^{C}Fe^{2+}$ increases for increasingly reducing conditions. FTIR data also provide strong evidence for slight but significant amounts of Li at the A sites.

Keywords Synthetic ferri-clinoholmquistite · Microprobe analysis · Infrared and Mössbauer spectroscopy · Structure refinement · Short-range order

G. Iezzi
Bayerisches GeoInstitut, University of Bayreuth, Germany

F. Cámara · R. Oberti
CNR-Istituto di Geoscienze e Georisorse, Sezione di Pavia, via Ferrata 1, 27100 Pavia, Italy

G. Della Ventura (✉)
Dipartimento di Scienze Geologiche, Università di Roma Tre, Largo S. Leonardo Murialdo 1, 00146, Roma, Italy
e-mail: dellaven@uniroma3.it
Tel.: +39-06-54888020
Fax: +39-06-54888201

G. Pedrazzi
Dipartimento di Sanità Pubblica, Sezione di Fisica, INFM Università di Parma, Via Volturno, 39, 43100 Parma, Italy

J-L Robert
ISTO, UMR 6113, 1A, Rue de la Férollerie, 45071 Orléans Cedex 2, France

Present address: G. Iezzi
Dipartimento di Scienze della Terra, Università di Chieti, I-66013 Chieti Scalo, Italy

Introduction

Holmquistites belong to the Mg-Fe-Mn-Li amphibole group, and have $^{B}Li > 1.00$ apfu (atom per formula unit) (Leake et al. 1997, 2003). They have been reported in about 30 localities all over the world (e.g. Deer et al. 1999), including the USA (Palache et al. 1930), the former USSR (Ginzburg et al. 1958; Gorelov et al. 1983), Canada (Nickel et al. 1960), Brazil (Lagache and Quéméneur 1997), Australia (Wilkins et al. 1970; Frost and Tsambourakis 1987), Africa (von Knorring and Hornung 1961), Sweden (Palache et al. 1930) and Italy (Borsi et al. 1978). Holmquistites typically occur at the contact of lithium-rich pegmatites with country rocks (Deer et al. 1999; London 1986), and their crystallization is mainly associated with metasomatic processes, where Li-rich amphiboles usually replace pre-existing spodumene or hornblende (Wilkins et al. 1970; Frost and Tsambourakis 1987; Shearer and Papike 1988; Lagache and Quéméneur 1997; Oberti et al. 2003).

^{B}Li amphiboles may crystallize with two different symmetries (orthorhombic *Pnma* and monoclinic $C2/m$). In the analogous ^{B}Mg system [$^{A}\square\,^{B}Mg_2\,^{C}Mg_5$ - $^{T}Si_8O_{22}(OH)_2$ - *Pnma* (anthophyllite) and $^{A}\square\,^{B}Mg_2\,^{C}Mg_5\,^{T}Si_8O_{22}(OH)_2$ - $P2_1/m$ or $C2/m$ (cummingtonite)], the change in symmetry is due to the Mg/Fe^{2+} ratio and/or to

the P, T conditions (cf. Boffa Ballaran et al. 2000, 2001 for references and detailed discussion). In ^{B}Li amphiboles, no rationale is provided for the phase transition, and very little is known about the stability of the various compositions. Iezzi et al. (2003a) described the synthesis and crystal-chemical characterization of end-member ferri-clinoferroholmquistite. In this paper we describe synthesis, crystal chemistry and crystal structure of ferri-clinoholmquistite, ideally $^{A}\square^{B}Li_2{}^{C}(Mg_3Fe^{3+}{}_2)^{T}Si_8O_{22}(OH)_2$. A combination of physically distinct analytical techniques, namely electron microprobe analysis (EMPA), X-ray powder diffraction (XPRD) and single-crystal structure refinement (SREF), infrared (FTIR), micro-Raman and Mössbauer spectroscopy has been used to characterize the run products. Each of these techniques has its own advantages and limitations. However, integration of long-range (EMPA, XPRD and SREF) and short-range information (FTIR and Mossbauer spectroscopy) is particularly fruitful for understanding all crystal-chemical mechanisms and details. This is particularly crucial when the results obtained on synthetic systems are applied to geological modelling, because the actual composition of synthetic amphiboles often deviates strongly from the nominal one, sometimes in a very subtle and totally unexpected manner.

Experimental

The starting material, used for all runs, was a silicate gel (Hamilton and Henderson 1968) having the composition of end-member ferri-clinoholmquistite, i.e. $\square Li_2(Mg_3Fe^{3+}{}_2)Si_8O_{22}(OH)_2$. This composition was run under different conditions; Table 1 lists experimental details and sample labels. Hydrothermal syntheses were done in internally heated pressure vessels. For runs at P = 0.4 GPa, the vessel was equipped with a Shaw membrane to control hydrogen fugacity (Scaillet et al. 1992), and the buffering conditions were imposed by an Ar–H_2 gas mixture (Gaillard et al. 2001; Scaillet et al. 1995). For the run at 0.55 GPa the same kind of vessel was used, with an intrinsic oxygen-buffering condition around NNO + 3 measured with the sensor method (Schmidt et al. 1997). The temperature was monitored by three sheathed type-K thermocouples located around the hot spot, the T gradient being within ± 5 °C. A transducer, calibrated against a Heise–Bourdon tube gauge, continuously recorded the pressure conditions; the estimated error is ± 2 MPa (Scaillet and Evans 1999).

Step-scan X-ray powder patterns were collected on a Scintag X1 diffractometer operated in the vertical θ–θ configuration with Ni-filtered CuKα radiation and a Si(Li) solid-state detector. Unit-cell dimensions were refined by whole-powder-pattern refinement (Rietveld method) using program DBW3.2 (Wiles and Young 1981).

FTIR spectra in the OH-stretching region (4000–3000 cm^{-1}) were collected at room T on a Nicolet 760 spectrophotometer equipped with a DTGS detector and a KBr beamsplitter. The nominal resolution is 4 cm^{-1}; spectra are the average of 64 scans. Samples were prepared as KBr pellets.

Electron-microprobe analyses were done at the Bayerisches Geoinstitut with a CAMECA SX-50 microprobe operating in the WDS mode, and under the following conditions: 15 kV excitation voltage, 10 nA beam current, 20 s counting time on peak and 10 s counting time on background. Minerals were used as standards: albite (Si, TAP), enstatite (Mg, TAP) and magnetite (Fe, LiF); data reduction was done with the PAP method (Pouchou and Pichoir 1985).

Suitable Mössbauer absorbers were obtained from finely powdered samples. The specimen mass was chosen in order to obtain a good signal-to-noise ratio while maintaining negligible thickness effects (Long et al. 1983; Rancourt et al. 1993). The samples were prepared as 0.3–0.4 mm thick sections, which give a total ^{57}Fe content of the order of 0.05 mg cm^{-2}. Mössbauer spectra were obtained at room temperature in transmission geometry using a 370 MBq ^{57}Co/Rh source and a constant-acceleration TAKES spectrometer coupled with a Wissel velocity transducer. The spectra were calibrated against SNP or metallic α-Fe foil. Isomer shifts (IS) are referred to room-temperature metallic α-Fe. The spectra were recorded using 512 channels of a multichannel analyzer, synchronized with the drive source (triangular waveform) in the velocity range ± 4 mm^{-1}s. Higher velocity ranges (± 10 mm^{-1}s) were also used in order to exclude the presence of hyperfine magnetic fields.

A single crystal 180 × 30 × 10 μm in size was hand-picked from the products of run 152 and analyzed using a Bruker-AXS SMART-Apex diffractometer working at 55 kV and 30 mA, with a crystal-to-detector distance of 5.0 cm and graphite-monochromatized MoKα X-radiation. A frame width of 0.2° in ω was used to collect 900 frames per batch in three batches at different φ values (0°, 120°, 240°); the counting time per frame was 60 s. Three-dimensional data were integrated and corrected for Lorentz, polarization and background effects using the SAINT + software version 6.02 (Bruker AXS). Data were collected up to θ = 30°, for a total of 3638 reflections (redundance up to 4), which were merged into

Table 1 Experimental conditions, sample labels and run products for nominal ferri-clinoholmquistite, $\square Li_2(Mg_3Fe^{3+}{}_2)Si_8O_{22}(OH)_2$. *Amp* amphibole; *qz* quartz; *cpx* Li-clinopyroxene; *up* unidentified phase

Sample	T (°C)	P (GPa)	Fugacity (log NNO)	Duration (days)	Run products (%) from Rietveld analysis
251	700	0.55	NNO + 3	12	amp (58), qz (14), cpx (28)
18a6	800	0.40	NNO + 1.5	7	amp (62), qz (10), cpx (28)
261	700	0.40	NNO + 1	12	amp (93), qz (7), up (< 1)
152	800	0.40	NNO	7	amp (92), qz (8), up (< 1)

1242 independent reflections yielding R_{sym} = 8.5% (4.6% for reflections with $I > 3\ \sigma_I$). Raw intensity data were corrected for absorption using the program SADABS v. 2.03 (Sheldrick 1996). Systematic extinctions were in agreement with space group $C2/m$. The structure refinement was done following the procedures discussed in Hawthorne et al. (1995). The unweighted full-matrix least-squares refinement on F was done with a program specifically written at the CNR-IGG-PV to deal with complex solid-solution terms. Only the reflections with $I \geqslant 2\ \sigma_I$ were considered as observed. Scattering curves for fully ionized chemical species were used at those sites where chemical substitutions occur; neutral vs. ionized scattering curves were used at the T and anion sites (cf. Hawthorne et al. 1995 and references therein). The final discrepancy factors are 7.9% for the 582 observed reflections and 18.1% for all the 1242 reflections. Atomic co-ordinates and displacement parameters are given in Table 2, selected interatomic distances and angles in Table 3, and lists of the observed and calculated structure factors are reported in Table 4, which has been deposited with the editor.

Table 3 Selected distances (Å) and angles (°) for crystal 152

T1–O1	1.607(13)	T2–O2	1.625(13)
T1–O5	1.606(12)	T2–O4	1.601(13)
T1–O6	1.620(12)	T2–O5	1.609(12)
T1–O7	1.614(6)	T2–O6	1.651(12)
<T1–O>	1.613	<T2–O>	1.622
V (Å^3)	2.151	V (Å^3)	2.178
TQE	1.0004	TQE	1.0033
TAV	1.66	TAV	13.47
M1–O1 × 2	2.067(13)	M2–O1 × 2	2.165(12)
M1–O2 × 2	2.115(12)	M2–O2 × 2	2.048(11)
M1–O3 × 2	2.076(13)	M2–O4 × 2	1.964(13)
<M1–O>	2.086	<M2–O>	2.059
V (Å^3)	11.884	V (Å^3)	11.440
OQE	1.0120	OQE	1.0133
OAV	39.56	OAV	41.46
M3–O1 × 4	2.093(12)	M4–O2 × 2	2.112(13)
M3–O3 × 2	2.070(18)	M4–O4 × 2	2.030(13)
<M3-O>	2.085	M4–O6 × 2	2.712(15)
V (Å^3)	11.807	<M4–O>	2.285
OQE	1.0159	V (Å^3)	11.595
OAV	51.28	O3–H	0.733(16)
T1–T1	3.061(8)	T1–T2	3.019(9)
T1–T2	3.090(9)		
T1–O7–T1	143.1	T1–O5–T2	139.80
T1–O6–T2	141.7	O5–O7–O5	127.2
O6–O7–O6	110.1	O5–O6–O5	171.0

TAV: tetrahedral angular variance,
TQE: tetrahedral quadratic elongation,
OAV: octahedral angular variance,
OQE: octahedral quadratic elongation.

Run products

Under reducing conditions ($\leqslant$ NNO + 1, Table 1), the amphibole yield is >90%, with minor quartz (7–8%, Table 1) as an additional phase. The X-ray powder patterns of samples 152 and 261 showed also the presence of very low-intensity peaks, due to some unidentified, very minor phase. Under oxidizing conditions ($\geqslant$ NNO + 1.5) the amphibole yield is low (<62%) and the assemblage is composed of amphibole ($\sim$ 30%) + abundant Li-bearing clinopyroxene (ferrispodumene: Cámara et al. 2003) + quartz.

It was observed that both the thermal and redox conditions significantly affect crystal size, the largest crystals being obtained at higher T and lower oxygen fugacity values. In run 152, the crystals are generally 2–8 μm wide and 10–40 μm long; a few crystals 30 μm wide and 180 μm long were observed (Fig. 1), and one of these was hand-picked for X-ray single-crystal data collection. Run 251, done under more oxidizing conditions (NNO + 3), yielded amphiboles with the smallest crystal size, on average 0.5–1 μm wide and 2–5 μm long; the other two runs (261 and 18a6) yielded amphibole crystals with intermediate sizes (Fig. 1).

Based on the structure refinement of sample 152, X-ray powder patterns of all run products were indexed in the $C2/m$ space group. The differences in the refined unit-cell parameters (Table 5) reflect the differences in composition (see below); the increase in the b edge and

Table 2 Atom coordinates, refined site-scattering values (ss, epfu), equivalent isotropic displacement parameters (Å^2) and anisotropic components (×10^4) of the displacement parameters for crystal 152

Site	ss	x/a	y/b	z/c	B_{eq}	β_{11}	β_{22}	β_{33}	β_{12}	β_{13}	β_{23}
O1		0.1145(13)	0.0879(6)	0.2067(27)	1.1	37(14)	6(4)	124(56)	7(5)	9(23)	−8(10)
O2		0.1225(13)	0.1725(5)	0.7238(26)	0.8	34(14)	1(3)	116(50)	0(5)	3(22)	4(9)
O3		0.1115(17)	0	0.7017(39)	1.0	18(18)	0(4)	238(95)	0	25(33)	0
O4		0.3760(13)	0.2487(6)	0.7705(27)	1.0	30(14)	7(3)	99(54)	−4(5)	8(22)	−3(10)
O5		0.3522(13)	0.1303(6)	0.0587(22)	0.9	28(13)	8(3)	52(45)	−1(5)	−23(20)	14(9)
O6		0.3481(13)	0.1189(6)	0.5583(23)	1.1	25(13)	14(4)	53(44)	11(5)	−1(20)	−20(10)
O7		0.3425(17)	0	0.2740(37)	1.1	36(20)	0(4)	229(80)	0	46(32)	0
T1		0.2883(5)	0.0852(2)	0.2723(11)	0.7	24(5)	2(1)	110(19)	1(2)	19(8)	−4(4)
T2		0.2978(5)	0.1702(2)	0.7835(11)	0.6	27(5)	2(1)	66(17)	−4(2)	9(8)	−3(3)
M1	29.6(4)	0	0.0883(3)	1/2	1.0	28(9)	2(2)	174(38)	0	20(13)	0
M2	38.6(4)	0	0.1811(2)	0	0.6	27(6)	2(1)	67(21)	0	15(8)	0
M3	14.8(3)	0	0	0	0.5	26(12)	3(3)	31(40)	0	5(16)	0
M4	19.2(4)	0	0.2566(6)	1/2	1.5	35(15)	8(3)	227(63)	0	44(22)	0
H	1.0	0.19	0	0.74	1.0						

Table 4 Can be supplied on request by the editor

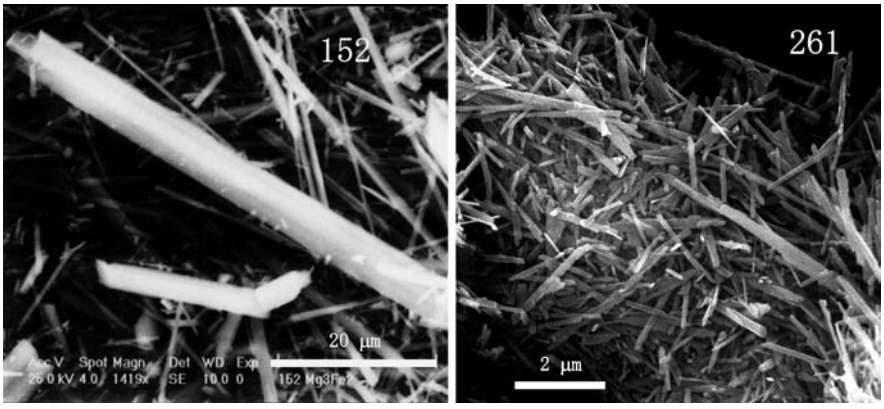

Fig. 1 *SEM-BSE* images of samples *152* and *261*. Note the *different size* of the scale bar

Table 5 Unit-cell parameters for ferri-clinoholmquistites synthesized under different conditions. X-ray powder for all samples and single-crystal (SC) data for sample 152. Samples arranged in order of decreasing f_{O_2}. FCFH ferri-clinoferroholmquistite data from Iezzi et al. (2003a)

Sample	a (Å)	b (Å)	c (Å)	β (°)	V (Å^3)
251	9.428(1)	17.878(3)	5.282(1)	102.06(2)	870.8(3)
18a6	9.446(1)	17.899(3)	5.288(1)	102.00(2)	877.6(6)
261	9.430(1)	17.872(3)	5.280(2)	101.84(3)	870.9(4)
152	9.474(1)	17.966(2)	5.292(1)	101.99(1)	881.1(2)
152 SC	9.466(2)	17.970(4)	5.288(1)	101.84(1)	880.4(1)
FCFH	9.484(3)	18.027(7)	5.321(1)	101.18(4)	892.7

unit-cell volume at low f_{O2}, in particular, is in accord with an increase in octahedral Fe^{2+}, and the value of the β angle is consistent with significant (Mg, Fe^{2+}) at M4. In addition, compared with end-member synthetic ferri-clinoferroholmquistite (Iezzi et al. 2003a, see Table 5), the unit-cell parameters measured for our amphiboles are consistent with the presence of a smaller octahedral divalent cation (Mg = 0.72 Å, Fe^{2+} = 0.78 Å: Shannon 1976) in the structure.

Mössbauer spectroscopy

Two run-powders, 152 and 261, consisting virtually of amphibole plus quartz only, were analyzed by Mössbauer spectroscopy (Fig. 2). Fitting of the data was performed by discrete site analysis using quadrupole doublets of Lorentzian lineshapes; each line of the doublet was constrained to have equal width and area.

Four doublets were used to adequately describe the resonance absorption patterns, and the refined parameters are given in Table 6. These doublets can be assigned to ferric and ferrous iron at the octahedral M1, M2, M3 and at the M4 sites (e.g. Iezzi et al. 2003a, b and references therein). The doublet with the largest quadrupole splitting (QS), i.e. 2.7–2.8 mm s^{-1}, is assigned to Fe^{2+} at the M1 site, that with QS in the range 2.4–2.5 mm s^{-1} is assigned to Fe^{2+} at the M3 site, and that with QS in the range 1.98–1.75 mm s^{-1} is assigned to Fe^{2+} at the M4 site (Hawthorne 1983; Redhammer and Roth 2002; Iezzi et al. 2003b). The doublet with the smallest isomer shift and QS around 0.25 mm s^{-1} is assigned to Fe^{3+} at the M2 site. The Fe^{2+}:Fe^{3+} ratios calculated from the fitted band intensities are 0.50:0.50 for sample 152, and 0.22:0.78 for sample 261 (Table 6). The results of the structure refinement of sample 152 (see below) show the presence of small amounts of Fe^{2+} at M2. The Fe^{2+}/Fe^{3+} content derived by Mössbauer for sample 152 is in close agreement with the Fe^{2+}/Fe^{3+} provided by SREF (see below).

Electron-microprobe analysis

Electron microprobe analyses of amphibole 152 are compared in Table 7 with the data calculated for stoichiometric ferri-clinoholmquistite. Two elements (H and Li) could not be analyzed, hence the crystal-chemical formula cannot be straightforwardly calculated from the available wt% oxides. However, given the experimental conditions and the amphibole composition system, the cation amounts can be calculated to give 8 Si and 2 H pfu, as discussed in Oberti et al. (2003). Moreover, the Fe^{3+}/Fe^{2+} ratio can be constrained to 0.50:0.50, as indicated by Mössbauer spectroscopy, and thus the Li content in apfu can be calculated to give electroneutrality in the unit formula. The B-site population can also be estimated by constraining $^{M4}Fe^{2+}$ to the value (21% of total Fe^{2+}) derived by Mössbauer spectroscopy. The data of Table 7 show a significant departure from the nominal stoichiometry, according to the coupled $^{C}(Mg,Fe^{2+})_1$ $^{B}(Mg,Fe^{2+})_1$ $^{C}Fe^{3+}{}_{-1}$ $^{B}Li_{-1}$ exchange vector, which has never been recorded so far in Li-bearing natural amphiboles. An odd feature in Table 7 is that a slight but significant amount of Li at the A site is necessary to achieve electroneutrality. The occurrence of ^{A}Li has never been reported so far for clino-amphiboles; how-

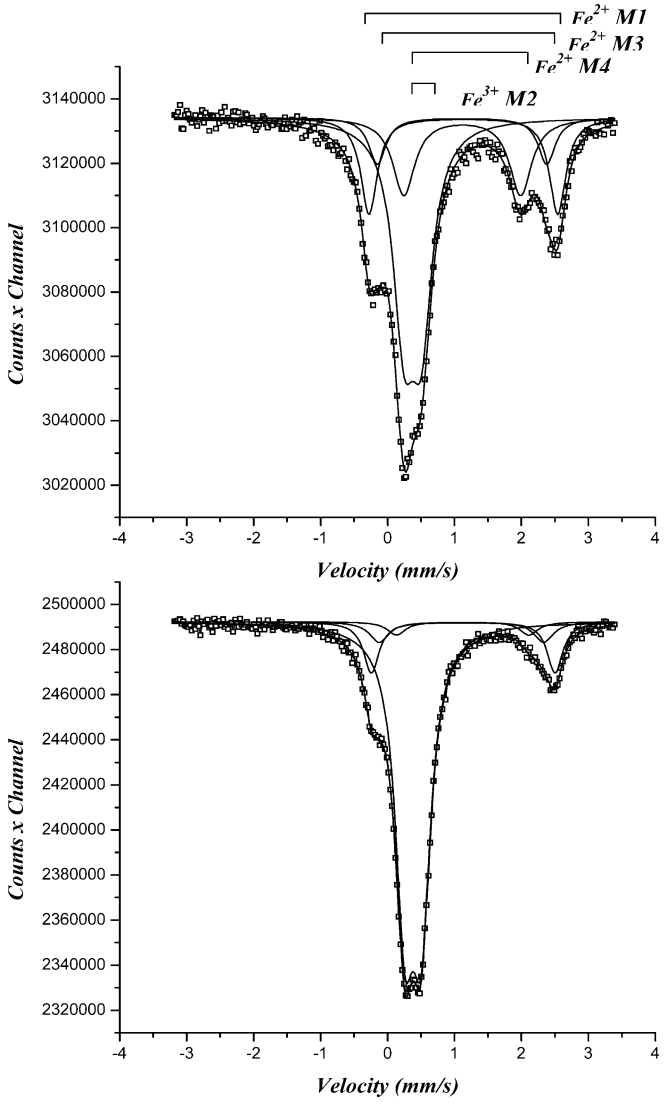

Fig. 2. Fitted Mössbauer spectra of samples 152 (*top*) and 261 (*bottom*)

ever, further support of this location is provided by IR analysis (see below).

It is worth noting that in terms of charge arrangement this synthetic composition is actually close to ferriwinchite, ideally $^{A}\square^{B}(NaCa)^{C}(Mg_4Fe^{3+})$ $Si_8O_{22}(OH)_2$. This arrangement has never been found in Mg–Fe–Mn–Li amphiboles, and is even not compatible with the present nomenclature scheme (Leake et al. 2003).

Table 7 EMP data for sample 152 (average of 20 points) and for ideal ferri-clinoholmquistite. Formulae calculated on the basis of 8 Si pfu and the constraints from Mössbauer analysis

Oxides	Ideal	152	apfu	Ideal	152
SiO_2	59.40	57.70	Si	8.00	8.00
Fe_2O_3	19.74	10.24[a]	Fe^{3+}	2.00	1.07
FeO	0.00	9.22[a]	Fe^{2+}	–	0.62
MgO	14.94	17.44	Mg	3.00	3.31
Li_2O	3.69	2.60[b]	Σ C	5.00	5.00
H_2O		2.16[b]	Mg	–	0.29
Total	100.00	99.36	Fe^{2+}	–	0.45
			Li	2.00	1.26
Ss calc at C	88.0	83.7	Σ B	2.00	2.00
Ss calc at B	6.0	19.0	^{A}Li	–	0.19
Ss calc at A	–	0.6	OH	2.00	2.00

[a] FeO/Fe_2O_3 from Mössbauer
[b] Calculated values

OH-stretching powder-IR spectroscopy

Description and interpretation of the spectra

OH-stretching spectra for the studied samples are shown in Fig. 3. As already discussed, runs 152 and 261 gave amphibole plus minor quartz, whereas runs 18a6 and 251 gave polyphase powders consisting of amphibole + pyroxene + quartz. Because the additional phases are all anhydrous, the IR spectrum in the OH region can be assigned to the amphibole only. Moreover, unreacted or not detected (amorphous) material, possibly present, if at all, in very low amounts as indicated by SEM + powder diffraction, are not likely to give IR bands in the high-frequency stretching range (>3600 cm^{-1}) studied here (e.g. Farmer 1974).

Ideal ferri-clinoholmquistite has only Mg at the OH-coordinated M(1,3) sites, and thus must have a single absorption band in the OH-stretching spectrum (e.g. Della Ventura 1992; Della Ventura et al. 1996; Hawthorne et al. 1996). This is not the case in Fig. 3, where only sample 251 shows a single-band pattern, whereas all other samples show up to four main bands at 3662,

Table 6 Mössbauer parameters for samples 152 and 261

Sample	Assignment	Isomer shift (mm s^{-1})	Quadrupole splitting (mm s^{-1})	FWHM (mm s^{-1})	Area (%)	χ^2
152	M1 Fe^{2+}	1.130(6)	2.814(18)	0.296(18)	19	1.04
	M3 Fe^{2+}	1.110(13)	2.525(40)	0.306(38)	10	
	M4 Fe^{2+}	1.11(48)	1.74(95)	0.398(22)	21	
	M2 Fe^{3+}	0.37(19)	0.26(38)	0.390(18)	50	
261	M1 Fe^{2+}	1.129(7)	2.743(22)	0.280(22)	12	1.00
	M3 Fe^{2+}	1.104(22)	2.456(79)	0.348(80)	6	
	M4 Fe^{2+}	1.122(37)	1.979(88)	0.326(95)	4	
	M2 Fe^{3+}	0.379(2)	0.248(3)	0.338(6)	78	

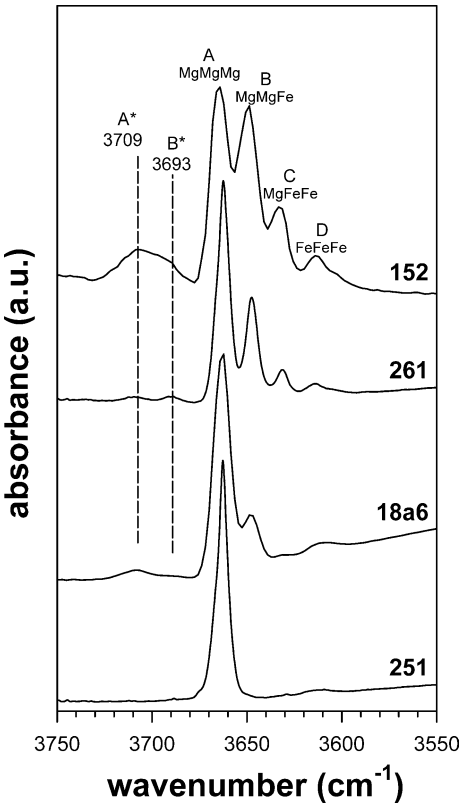

Fig. 3 OH-stretching IR spectra for the studied samples

3648, 3631 and 3614 cm^{-1}, respectively; these bands are denoted A to D in Fig. 3. The single band at 3662 cm^{-1} in the spectrum of sample 251 (Fig. 3, bottom) can be assigned to the $^{M1}Mg^{M1}Mg^{M3}Mg$–OH–$^{A}\square$-[^{M4}Li] configuration; the analogous band in tremolite, $^{M1}Mg^{M1}Mg^{M3}Mg$–OH–$^{A}\square$-[^{M4}Ca], is found at 3675 cm^{-1} (e.g. Hawthorne et al. 1997). Given the same NN (nearest-neighbour) configuration between tremolite and ferri-clinoholmquistite, the reason for the observed frequency shift ($\Delta_v = -13$ cm^{-1}) must be ascribed to a NNN (next-nearest-neighbour) effect, probably a combination of the presence of Fe^{3+} at the M2 site and of Li at the M4 site. Iezzi et al. (2003a) found a shift of -10 cm^{-1} between the Fe–Fe–Fe–OH–$^{A}\square$ band in synthetic ferri-clinoferroholmquistite (^{M4}Li and $^{M2}Fe^{3+}$ = 2.0 apfu) and actinolite (^{M4}Ca and $^{M2}Fe^{2+}$ = 2.0 apfu).

The A–D components can be assigned to distinct combinations of Mg and Fe^{2+} at the M1 and M3 sites (e.g. Della Ventura et al. 1996), as shown schematically in Fig. 3. Sample 152 shows, in addition to the A–D bands, two broad and overlapping absorptions in the 3693–3709 cm^{-1} region, which can also be detected in samples 261 and 18a6 (Fig. 3).

Assignment of the bands at 3693 and 3709 cm^{-1}

The assignment of the two broad, minor absorptions at 3693 and 3709 cm^{-1} is not straightforward. There are some points which are relevant here: (1) these bands are a real feature of the amphibole spectrum; in fact, micro-Raman spectroscopy on single crystals hand-picked from sample 152 (courtesy of J.-M. Bény, Orléans) gave the same pattern as shown in Fig. 3, thus excluding the possibility that they belong to additional and non-identified phases in the bulk run-powder used to prepare the KBr disk for IR analysis; (2) the 3693 and 3709 cm^{-1} bands are shifted toward higher frequency with respect to the A–D quartet of bands, and hence can be associated solely with either the presence of a monovalent cation at the M3 site or with partial A-site occupancy (e.g. Della Ventura et al. 2003; Iezzi et al. 2003b).

The IR spectrum of sample 152 is compared in Fig. 4 with that of a synthetic amphibole solid solution along the magnesioriebeckite ($\square Na_2Mg_3Fe^{3+}{}_2Si_8O_{22}OH_2$) – magnesioarfvedsonite ($NaNa_2Mg_4Fe^{3+}Si_8O_{22}OH_2$) join (sample 313, from Della Ventura et al. in preparation). The two spectra are very similar, and both show a quadruplet of sharp bands at frequencies < 3670 cm^{-1}, and a broad absorption at frequencies > 3670 cm^{-1}. The four sharp bands have the same frequency and almost identical relative intensity, suggesting that both amphiboles have similar Mg–Fe^{2+} distribution at the M1 and M3 sites. In sample 313, the A*–D* quadruplet can be assigned to the $^{M(1,3)}$(Mg–Fe^{2+})–OH–^{A}Na local environments. Thus also the broad bands at 3693 and 3709 cm^{-1} can be confidently assigned to A-site-occupied environments and, given the controlled chemistry of the system, the only suitable candidate for A-site occurrence is Li. In this model, the 3709 cm^{-1} band (A* in Fig. 4) is associated with MgMgMg–OH–^{A}Li, whereas the 3693 cm^{-1} band (B in Fig. 4) is associated with MgMgFe–OH–^{A}Li; in the case of sample 152, the C* and D* bands, associated with the MgFeFe–OH–^{A}Li and the FeFeFe–OH–^{A}Li environments, are invisible due to their low intensity and/or complete overlap with the A and B bands.

Previous work (e.g. Della Ventura 1992; Hawthorne et al. 1997) shows that the shift from a vacant A-site environment induced by ^{A}K is similar but not equal to that induced by ^{A}Na ($\Delta v = +60$ cm^{-1} vs. $+55$ cm^{-1}); this difference is due to a combination of several effects, such as the cation size and ordering pattern, which both control the extent of the A^+–H^+ local interaction. Figure 4 suggests that the shift due to ^{A}Li is close to $+50$ cm^{-1}. The amount of ^{A}Li can be estimated by considering the difference in molar absorptivity (Skogby and Rossman 1991) between vacant and occupied A-site environments. According to Hawthorne et al. (1997), the molar fraction of A-site vacant environments ($X_\square$) can be derived from the relative intensity of the bands in the IR spectrum using the equation $X_\square = R/[k + R(1\text{-}k)]$, where R is the measured relative intensity ratio between the A-site vacant and the A-site filled environment, and k is the correction factor for the difference in molar absorptivity ($k = 2.2$ in the tremolite-richterite system:

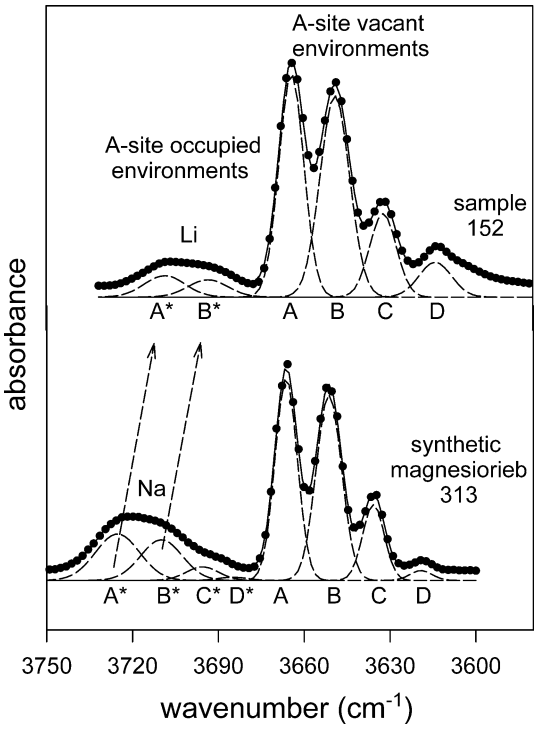

Fig. 4 The fitted OH-stretching spectrum of sample 152 compared to the spectrum of synthetic magnesioriebeckite 313 (Della Ventura et al., unpublished data). The *band labels* are also indicated (see text)

Hawthorne et al. 1997). Using this equation, the calculated contents of ^{A}Li are 0.20, 0.06, and 0.04 apfu for samples 152, 261 and 18a6, respectively. For sample 152, this estimate is coherent with the recalculation of the EMP analysis, which also supports the use of $k = 2.2$ in this system.

Calculation of the aggregate M(1,3) site occupancies

The intensities of the A–D bands (Fig. 3) are related to the frequency of occurrence of each octahedral Mg-Fe^{2+} configuration, thus providing a way to quantify the Mg–Fe^{2+} content at the aggregate M1 and M3 sites using the equations of Burns and Strens (1966):

$$Mg_{M(1,3)} = 3I_A + 2I_B + I_C$$

$$M^{2+}_{M(1,3)} = I_B + 2I_C + 3I_D \ ,$$

where $I_{A\text{-}D}$ are the intensities of the A to D bands (e.g. Della Ventura et al. 1996; Hawthorne et al. 1996). The digitized spectra were fitted (Fig. 4) by interactive optimization followed by least-squares refinement (Della Ventura et al. 1996); the background was treated as linear and all bands were modelled as symmetric Gaussians (Strens 1974). The results obtained for the studied samples are given in Table 8. For samples 152, 261 and 18a6, the situation is somewhat complicated by the fact that some (Mg, Fe^{2+}) is associated with ^{A}Li; however, since the number of ^{A}Li environments can be estimated (see above) the total amount of octahedral (Mg, Fe^{2+}) can also be calculated (Table 8).

The effect of the M4 site populations on the IR spectra

Different NNN environments around the OH group give rise to significant band broadening, and eventually to new bands in the OH-stretching spectrum. This aspect is still not fully understood, but several data accumulated during the last few years on synthetic compositions show that the B-site occupancy of amphiboles significantly affects the principal OH-stretching bands. For example, Gottschalk et al. (1999) and Hawthorne et al. (2000) showed that in tremolite even slight amounts of ^{B}Mg (substituting for ^{B}Ca) produce a minor but well-defined new band which is shifted 7–8 cm^{-1} downward from the main absorption. Iezzi et al. (2003b) showed that in ferri-clinoferroholmquistite the main OH band broadens and shifts linearly by 4 cm^{-1} as a consequence of the Na_1 Li_{-1} substitution at the B sites.

Figure 5a shows that the single band of sample 251 is broader and strongly asymmetric when compared with the single band of synthetic tremolite, suggesting the presence of one additional and partly overlapping component around 3668 cm^{-1}. This component can be assigned to a small divalent cation at the B sites, i.e. to the $^{M1}Mg^{M1}Mg^{M3}Mg$–OH–$^{A}\square$–[^{M4}(Fe,Mg)] configuration, because this is the frequency typical of cummingtonite (Boffa Ballaran et al. 2001) and of the cummingtonite component in tremolite (e.g. Hawthorne et al. 2000). Given the controlled chemistry of the system and the presence of a single band in the IR spectrum, the only available charge-balance substitution for the entry of a divalent cation at the B sites is the simultaneous entry of a divalent cation substituting for Fe^{3+} at the M2 site. The crystal-chemical formula of sample 251 can thus be expressed as $\square(Li_{2-x}M^{2+}{}_x)(M^{2+}{}_{3+x}Fe^{3+}{}_{2-x})Si_8O_{22}(OH)_2$, with M1 = 2.0 Mg and M3 = 1.0 Mg. A crude estimation done by fitting two components to the spectrum of Fig. 5a provides $x \sim 0.20$ apfu. Figure 5b shows an enlargement of all recorded IR spectra in the region 3640–3680 cm^{-1}, where it is apparent that a second component at $\sim$ 3668 cm^{-1} is observed with different intensity in all studied samples. For sample 152, in particular, the 3662 and 3668 cm^{-1} components have the same intensity; this feature supports the assignment of

Table 8 Site populations (apfu) at the M(1,3) and A sites as derived by FTIR spectroscopy

Sample		251 IR	18a6 IR	261 IR	SREF	152 EMPA Möss.	IR
$\Sigma_{M1,3}$	Mg	3.00	2.82	2.69	2.40	2.38	2.21
	Fe^{2+}	0.00	0.16	0.31	0.60	0.62	0.79
^{A}Li		0.00	0.04	0.06	n.d.	0.19	0.20

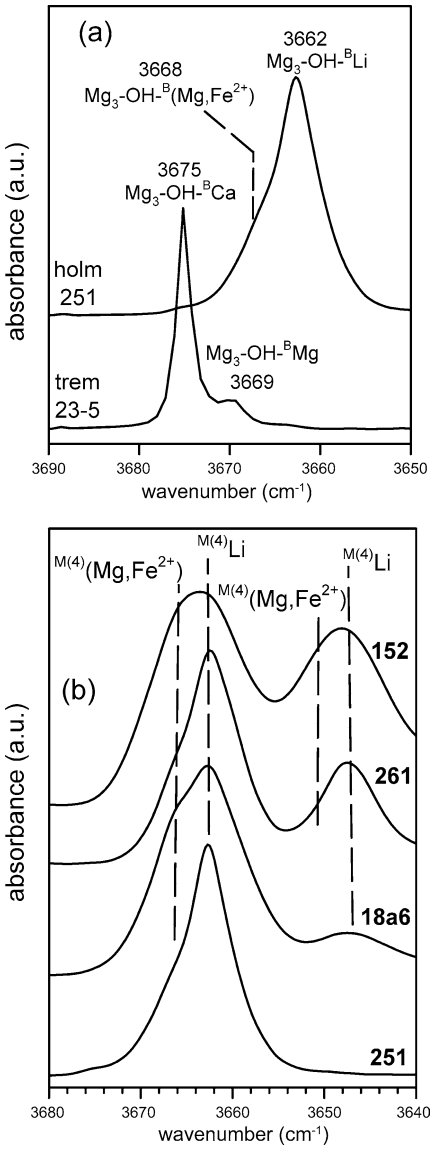

Fig. 5 a The IR spectrum of sample 152 compared with the spectrum of synthetic tremolite 23–5 (Hawthorne et al. 2000). **b** Enlarged IR spectra for all synthesized amphiboles. The *band assignments* are indicated.

the 3668 cm^{-1} band to the $^{M1}Mg^{M1}Mg^{M3}Mg$–OH–$^{A}\square$–[^{M4}(Fe,Mg)] configuration because both EMP and Mössbauer analysis show that sample 152 has $^{B}Li \sim {}^{B}(Mg, Fe^{2+})$. Due to the several problems associated with the decomposition of these spectra, we cannot use the relative intensities of the 3662 and 3668 cm^{-1} components for quantitative purposes; however, the spectra of Fig. 5b allow us to conclude that all synthesized amphiboles have significant (Mg, Fe^{2+}) at M4. It must be stressed that similar components, shifted upward and associated with the main absorption, have been observed in both natural (Law and Whittaker 1981) and synthetic holmquistites (Iezzi et al., in preparation).

Cation order from structure refinement of sample 152

The refined <T1–O> and <T2–O> bond distances (1.613 and 1.622 Å, respectively) confirm that only Si is present in the tetrahedral sites. The site-scattering values refined at the B- and C-group sites are in good agreement with those calculated from the analysis reported in Table 7. The M1 and M3 sites are occupied only by divalent cations, and the proposed site populations are $^{M1}(Mg_{1.60}Fe^{2+}{}_{0.40})$ and $^{M3}(Mg_{0.80}Fe^{2+}{}_{0.20})$, which implies Fe^{2+}/Mg disorder. No evidence of the occurrence of Li at the M3 site was detected. At the M2 site, the refined site-scattering value is coherent with $Fe_{1.04}Mg_{0.96}$, but the mean bond length (which is longer than expected) suggests that a small fraction of Fe is in the divalent state. This latter feature could not be detected by Mössbauer analysis. The *y* coordinate of the M4 site is that expected for a site population with only small cations, such as Li, Mg, and Fe^{2+} (Oberti et al. 2003). Accordingly, the co-ordination is [4 + 2]-fold, with the two O5 anions being out of the co-ordination sphere (Table 3). This feature implies the need for further bond-strength contribution on the O5 anion, which, for an essentially A-site-vacant amphibole, must be provided by the tetrahedral cations; actually, the observed T1–O5 and T2–O5 distances are quite short (Table 3).

Given the EMP and FTIR evidence suggesting the occurrence of Li at the A sites, the difference-Fourier map of sample 152 was analyzed very carefully. Li is far smaller than Na and K ($^{[8]}$i.r. = 0.92, 1.18 and 1.51 Å, respectively; Shannon 1976), and thus its occurrence in the usual A sites (A*m* and A2) is very unlikely. Among the highest 20 residuals in the difference-Fourier map, four can be explained as Si–O-bonding electrons (a common feature in amphiboles and pyroxenes); they peak at 2.1, 1.9, 1.9 and 1.8 electrons $Å^{-3}$, respectively. Another residual (1.8 electrons $Å^{-3}$) falls in the A cavity at coordinates 0 0.44 1/2 (A2), and has a very distorted tetrahedral co-ordination with two O6 and two O7 sites. This residual has an average distance of 1.94 Å with the surrounding O atoms, which might be suitable for Li ($^{[4]}$i.r. = 0.59; Shannon 1976). Due to local symmetry, this position repeats itself in the A cavity at a distance of 2.156 Å. The maximum site scattering corresponding to full ^{A}Li occupancy is 1.5 epfu, making the detection by SREF very difficult, especially when dealing with small crystals and low occupancies, as is the case for sample 152.

Discussion and conclusions

Although the phase relationships in the studied system have not been fully bracketed, ferri-clinoholmquistite is known to have a thermal stability about 300 °C higher than ferri-clinoferroholmquistite, for a large range of pressure (0.1–0.7 GPa) (Iezzi 2001). The present work

suggests that oxygen fugacity is a key parameter in controlling the amphibole composition. End-member ferri-clinoholmquistite, ideally $\square Li_2Mg_3Fe^{3+}{}_2Si_8O_{22}(OH)_2$, is stable only under very oxidizing conditions (close to NNO + 3). Under more reducing conditions, the amphibole invariably contains Fe^{2+} at the M1 and M3 sites, as well as at the M4 sites. Reducing conditions of synthesis also promote the entry of slight but significant amounts of ^{A}Li into the amphibole structure.

The present work confirms that Fe^{3+} is strongly ordered at the M2 site in synthetic ferri-clinoholmquistite, whereas Fe^{2+} is disordered over the M1, M3 and M4 sites. This result is coherent with the conclusions drawn by the extensive crystal-chemical study of Li-bearing amphiboles found in metamorphic episyenites from the Pedriza Massif, Spain (cf. Oberti et al. 2003 for a review). However, in the natural and more complex systems, the $^{M4}(Mg,Fe^{2+})_1{}^{M4}Li_{-1}$ exchange was never observed, the solid solution at M4 being ruled by the homovalent exchange $^{M4}Na_1{}^{M4}Li_{-1}$. Although all synthetic amphiboles of this work must be classified as ferri-clinoholmquistites in the present nomenclature scheme, because ^{B}(Fe,Mg,Mn,Li) $\geqslant$ 1 and ^{B}Li $\geqslant$ 1.0 apfu: Leake et al. 1997, 2003), they approach a totally new arrangement for the ^{B}(Fe,Mg,Mn,Li) amphibole group, i.e. $^{B}[(Mg, Fe)^{2+}{}_1Li_1]$. If a similar composition were found in nature, it would deserve a new root name.

The present study also provides evidence for another very unusual feature for amphibole crystal chemistry: the possibility for a small monovalent cation, such as Li, to enter the A site. The presence of ^{A}Li was suggested long ago in the orthorhombic *Pnmn* protoamphibole by Gibbs (1962) on the basis of chemical analysis. However, his structure refinement based on three-dimensional X-ray diffraction data collected with a Weissenberg camera did not provide any evidence of A cations. Some crystal chemical features, such as the relative lengths of the O–O edges of the tetrahedra, suggested that Li could coordinate the O5 and O7 oxygen atoms (Gibbs 1969). Li at the A site was inferred by Maresch and Langer (1976) on the basis of the bulk analysis of the starting gels in a very peculiar amphibole with orthorhombic P*nma* symmetry synthesized in the Li_2O–MgO–SiO_2–H_2O system. Robert (1981) experimentally investigated the distribution of Li^+ between pargasite $[NaCa_2(Mg_4Al)(Si_6Al_2)O_{22}(OH)_2]$ and hydrothermal LiCl solutions, and suggested the possible replacement of Na^+ by Li^+ at the A site at 600 °C and 1 *K*bar; however, no direct crystal-chemical information could be obtained on the synthesized phases. The spectroscopic (IR + Raman) data presented here provide for the first time reliable spectroscopic evidence for the occurrence of Li at the A site in amphiboles.

Due to crystal size, sample 152 could be characterized with all the techniques used for this work. Although its composition is the farthest from nominal ferri-clinoholmquistite, it is a key sample to check for the consistency of the different analytical approaches. The conclusion is that spectroscopic methods, particularly when used in combination (e.g. FTIR + Mössbauer), provide a reliable crystal-chemical characterization (Table 8) of fine-grained synthetic products.

The intriguing point which emerges from the presented work is that under very oxidizing conditions the amphibole yield is very low but its composition is close to that of the starting bulk system, whereas the reverse is true for reducing conditions. The low amphibole yield is in accord with the fact that, in the Li-rich system investigated here, oxidizing conditions favour crystallization of clinopyroxene (ferri-spodumene close to $LiFe^{3+}Si_2O_6$ in our case: Cámara et al. 2003) as already observed for alkali-rich systems in general (e.g. Scaillet and McDonald 2001). However, due to the strong predominance of Fe^{3+} in the system at these conditions, the $^{C}(Mg,Fe^{2+})_1{}^{B}(Mg,Fe^{2+})_1{}^{C}Fe^{3+}{}_{-1}{}^{B}Li_{-1}$ exchange vector is minimized, and the composition of the amphibole must be very close to the nominal one. Reducing conditions favour the crystallization of the amphibole over pyroxene, but make operative the $^{C}(Mg,Fe^{2+})_1{}^{B}(Mg,Fe^{2+})_1{}^{C}Fe^{3+}{}_{-1}{}^{B}Li_{-1}$ exchange, and the amphibole composition diverges from the expected stoichiometry. In other words, the amphibole structure is flexible enough to compensate for large compositional variations of the system, and its composition is ultimately controlled by crystal-chemical rules, such as local charge arrangements.

Acknowledgements Sergio Lomastro assisted with powder XRD data collection, and Jean-Michel Bény collected the microRaman spectrum of sample 152. This work was initiated during the PhD of GI at I.S.T.O.-C.N.R.S. (Orléans), which was funded by the University of Chieti and an EGIDE-French Foreign Affairs Ministry fellowship. Part of the work was also done during the stay of GDV at the Museum d'Histoire Naturelle, Paris, thanks to a grant from MNHN, Minéralogie, Paris. Constructive criticism from Fritz Seifert, Annibale Mottana, and two anonymous referees helped to improve the clarity of the text. The post-Doc stay of G.I at Bayerisches Geointitut was financed by a Sofia Kovacevskaja Program.

References

Boffa Ballaran T, Angel RJ, Carpenter MA (2000) High-pressure transformation behaviour of the cummingtonite-grunerite solid solution. Eur J Mineral 12: 1195–1213

Boffa Ballaran T, Carpenter MA, Domeneghetti MC (2001) Phase transition and mixing behaviour of the cummingtonite-grunerite solid solution. Phys Chem Miner 28: 87–101

Borsi S, Del Moro A, Sassi FP, Zanferrari A, Zirpoli G (1978) New geopetrologic and radiometric data on the alpine history of the Austridic continental margin south of the Tauern window. Memorie Scienze Geologiche 32: 1–17

Burns RG, Strens RGJ (1966) Infrared study of the hydroxile bonds in clinoamphiboles. Science 153: 890–892

Cámara F, Iezzi G, Oberti R (2003) HT-XRD study of synthetic ferrian magnesian spodumene: the effect of site dimension on the $P2_1/c \rightarrow C2/c$ phase transition. Phys Chem Miner 30: 20–30

Deer WA, Howie RA, Zussman, J (1999) Rock forming minerals. Double-chain silicates. Ed. Longman Scientific & Technical, New York pp 692

Della Ventura G (1992) Recent developments in the synthesis and characterization of amphiboles. Synthesis and crystal chemistry of richterite. Trends Mineral 1: 153–192

Della Ventura G, Robert JL, Hawthorne FC (1996) Infrared spectroscopy of synthetic (Ni,Mg,Co)-potassium-richterite. In Dyar MD, McCammon C, Schaefer M. W (eds) Mineral spectroscopy : a tribute to Roger G. Burns. pp. 55–63. The Geochemical Society Special Publication No. 5

Della Ventura G, Hawthorne FC, Robert JL, Iezzi G (2003) Synthesis and infrared spectroscopy of amphiboles along the tremolite – pargasite join. Eur J Mineral 15: 341–347

Farmer VC (1974) The infrared spectra of minerals. The Mineralogical Society, of America, Washington, DC Monograph 4, pp 539

Frost MT, Tsambourakis G (1987) Holmquistite-bearing amphibolite from Greenbushes, Western Australia. Min Mag 51: 585–591

Gaillard F, Scaillet B, Pichavant M., Beny JM (2001) The effect of water and fO_2 on the ferric-ferrous ratio of silicic melts. Chem Geol 174: 255–273

Gibbs GV (1962) The crystal structure of protoamphibole. PhD Thesis, Pennsylvania State University, University Park, Pa

Gibbs GV (1969) The crystal structure of protoamphibole. Mineralogical Society of America, Washington DC, Special Paper 2: 101–110

Ginzburg IV, Rogachev DL, Bondareva AM (1958) New data on holmquistite (in Russian). Dokl Akad Nauk SSSR 119: 1013–1016

Gorelov GF, Gorb AM, Kosukhina IG, Sofanov AM, Shestakov AV (1983) Holmquistite from Tarynnakhsky ferruginous quarzite locality, Charo-Takkinsky area (Aldan Shield), (in Russian). Geolog Geofiz 2: 129–131

Gottschalk M, Andrut D, Melzer S (1999) The determination of the cummingtonite content of synthetic tremolite. Eur J Mineral 11: 967–982

Hamilton DL, Henderson CMB (1968) The preparation of silicate compositions by a gelling method. Min Mag 36**:** 832–838

Hawthorne FC (1983) The crystal chemistry of the amphiboles. Can Mineral 21: 173–480

Hawthorne FC, Ungaretti L, Oberti R (1995) Site populations in minerals: terminology and presentation of results of crystal-structure refinement. Can Mineral 33: 907–911

Hawthorne FC, Della Ventura G, Robert JL (1996) Short-range order and long-range order in amphiboles: a model for the interpretation of infrared spectra in the principal OH-stretching region. Geochim Cosmochim Acta, Special vol 5: 49–54

Hawthorne FC, Della Ventura G, Robert JL, Welch MD, Raudsepp M, Jenkins DM (1997) A Rietveld and infrared study of synthetic amphiboles along the potassium–richterite–tremolite join. Am Mineral 82: 708–716

Hawthorne FC, Welch MD, Della Ventura G, Shuangxi L, Robert JL, Jenkins DM (2000) Short-range order in synthetic aluminous tremolites: an infrared and triple-quantum MAS NMR study. Am Mineral 85: 1716–1724

Knorring von O, Hornung G (1961) On the lithium amphibole holmquistite, from Benson pegmatite mine, Mtoko, Southern Rhodesia. Min Mag 32: 731–735

Iezzi G (2001) Cristallochimie des amphiboles à lithium, approche expérimentale. Unpub PhD Thesis, University of Orléans, France

Iezzi G, Della Ventura G, Pedrazzi G, Robert JL, Oberti R (2003a) Synthesis and characterisation of ferri-clinoferroholmquistite, $\square Li_2(Fe^{2+}{}_3Fe^{3+}{}_2)Si_8O_{22}(OH)_2$. Eur J Mineral 15: 321–327

Iezzi G, Della Ventura G, Cámara F, Pedrazzi G, Robert JL (2003b) The ^{B}Na–^{B}Li exchange in A-site vacant amphiboles: synthesis and cation ordering along the ferri-clinoferroholmquistite–riebeckite join. Am Mineral 88: 955–961

Lagache M, Quéméneur J (1997) The Volta Grande pegmatites, Minas Gerais, Brazil: an example of rare-element granitic pegmatites exceptionally enriched in lithium and rubidium. Can Mineral 35: 153–165

Law AD, Whittaker EJ (1981) Studies of the orthoamphiboles 1. The Mössbauer and infrared spectra of holmquistite. Bull Mineral 104: 381–386

Leake BE, Woolley AR, Arps CES, Birch WD, Gilbert MC, Grice JD, Hawthorne FC, Kato A, Kisch HJ, Krivovichev VG, Linthout K, Laird J, Mandarino JA, Maresch WV, Nickel EH, Rock NMS, Schumacher JC, Smith DC, Ungaretti L, Whittacker EJW, Youzhi G (1997) Nomenclature of amphiboles: report of the subcommittee on amphiboles of the International Mineralogical Association, commission on new minerals and minerals names. Eur J Mineral 9: 623–651

Leake BE, Woolley AR, Birch WD, Burke EAJ, Ferraris G, Grice JD, Hawthorne FC, Kisch HJ, Krivovichev VG, Schumacher JC, Stephenson NCN, Whittaker EJW (2003) Nomenclature of amphiboles: additions and revisions to the International Mineralogical Association's amphibole nomenclature. Can Mineral 41: 1355–1362

London D (1986) Holmquistite as a guide to pegmatitic rare metal deposits. Econ Geo 81: 704–712

Long G, Cranshaw TE, Longworth G (1983) The ideal Mössbauer effect absorber thickness. Möss Eff Ref Data J 6(2): 42–49

Maresch WV, Langer K (1976) Synthesis, lattice constants and OH-valence vibrations of an orthorhombic amphibole with excess OH in the system Li_2O–MgO–SiO_2–H_2O. Contrib Mineral Petrol 56: 27–34

Nickel EH, Karpoff BS, Maxwell JA, Rowland JF (1960) Holmquistite from Barraute, Quebec. Can Mineral 6: 504–512

Oberti R, Cámara F, Ottolini L, Caballero JM (2003) Lithium in amphiboles: detection, quantification, and incorporation mechanisms in the compositional space bridging sodic and ^{B}Li-amphiboles. Eur J Mineral 15: 309–319

Palache C, Davidson SC, Goranson EA (1930) The hiddenite deposit in Alexander County, North Carolina. Am Mineral 15: 280–302

Pouchou JL, Pichoir F (1985) "PAP" Ø(ρZ) procedure for improved quantitative micro-analysis. Microbeam Anal 104–160

Rancourt DG, McDonald AM, Lalonde AE, Ping JY (1993) Mössbauer absorber thickness for accurate site populations in Fe-bearing minerals. Am Mineral 78: 1–7

Redhammer GJ, Roth G (2002) Crystal structure and Mössbauer spectroscopy of the synthetic amphibole potassic ferri-ferro-richterite at 298 K and low temperatures (80–110 K). Eur J Mineral 14: 105–114

Robert JL (1981) Etudes cristallochimiques sur les micas et les amphiboles. Applications à la pétrographie et à la géochimie. Thèse d'Etat, Université Paris-Sud, Orsay, N° d'Ordre 2408, 206 pp

Scaillet B, Evans BW (1999) The June 15, 1991 eruption of Mount Pinatubo: I. Phase equilibria and pre-eruption P–T–fO_2–fH_2O conditions of the dacite magma. J Petrol 40: 381–411

Scaillet B, McDonald R (2001) Phase relations of peralkaline silicic magmas and petrogenetic implications. J Petrol 42: 825–845.

Scaillet B, Pichavant M, Roux J, Humbert G, Lefevre A (1992) Improvements of the Shaw membrane techniques for measurements and control of fH_2 at high temperatures and pressure. Am Mineral 77: 647–655

Scaillet B, Pichavant M, Roux J (1995) Experimentally crystallisation of leucogranite magmas. J Petrol 36: 663–705

Schmidt BC, Holtz F, Scaillet B, Pichavant M (1997) The influnce of H_2O–H_2 fluids and redox conditions on melting temperatures in the haplogranite system. Contrib Mineral Petrol 126**:** 386–400

Shannon RD (1976) Revised effective ionic radii and systematic studies of interatomic distances in halides and chalcogenides. Acta Crystallogr A32: 751–767

Shearer CK, Papike JJ (1988) Pegmatite–wall rock interaction: holmquistite-bearing amphibolite, Edison pegmatite, Black Hills, South Dakota. Am Mineral 73: 324–337

Sheldrick GM (1996) SADABS, Siemens area detector absorption correction software. University of Göttingen, Germany

Skogby H, Rossmann GR (1991) The intensity of amphibole OH bands in the infrared absorption spectrum. Phys Chem Miner 18: 64–68

Strens RSJ (1974) The common chain, ribbon and ring silicates. In: Farmer VC (ed) The infrared spectra of minerals Mineralogical Society of America, Washington, DC, Monograph 4:305–330

Wiles DB, Young PA (1981) A new computer program for Rietveld analysis of X-ray powder diffraction patterns. J Appl Cryst 14: 149–151

Wilkins RW, Davidson LR, Ross JR (1970) Occurrence and infrared spectra of holmquistite and hornblende from Mt. Marion, near Kalgoorlie, Western Australia. Contrib Mineral Petrol 28: 280–287